# Molecular interactions in the condensed phases of ortho-para hydrogen mixtures*

P. A. Fleury
*Bell Laboratories, Murray Hill, New Jersey 07974*

J. P. McTague†
*Bell Laboratories, Murray Hill, New Jersey 07974*
*and Chemistry Department,‡ University of California, Los Angeles, California 90024*

(Received 18 November 1974; revised manuscript received 3 April 1975)

Because mixtures containing arbitrary ratios of ortho ($J = 1$) and para ($J = 0$) concentrations can be prepared, the condensed phases of hydrogen afford a unique opportunity to study interactions between isotropic and anisotropic molecules which are chemically identical. Detailed measurements are reported here of the rotational Raman spectra in the liquid and solid phases of ortho-para hydrogen mixtures, with para concentrations between 25% and 96% at temperatures between 10 and 23 °K. Changes in the configuration and dynamics of the molecular environment with temperature and ortho concentration are clearly reflected in the rotational Raman line shapes. Logarithmically recorded spectra, covering an intensity dynamic range of typically $10^4$, reveal two relatively independent types of interaction which respectively govern the near ($<30$ cm$^{-1}$) and far ($>30$ cm$^{-1}$) wings. Quantum calculations of the low-frequency mechanism, electric quadrupole-quadrupole molecular pair interactions, are presented. They are found to produce values for the second frequency moments for all three ($J = 1\rightarrow 1$, $J=1\rightarrow 3$, and $J=0\rightarrow 2$) rotational transitions which agree well both in absolute magnitude and in concentration dependence with experimental observations. The far wings in the solid spectra consist of phonon sidebands whose structure is in good agreement with the phonon density of states previously observed by neutron scattering. In the liquid mixtures the far-wing line shapes are insensitive to temperature or concentration variation and are very similar to the solid wings.

## I. INTRODUCTION

The line shapes of rotational Raman transitions—which would be $\delta$ functions for stationary noninteracting molecules—contain information on the configuration and dynamics of the molecular environment in a condensed phase.[1] Because it can be prepared in an arbitrary mixture of ortho ($J=1$) and para ($J=0$) concentrations, molecular hydrogen provides a unique opportunity to study such effects as the interactions between isotropic and anisotropic molecules which are chemically identical. In this paper we present the results of such a study based on the rotational Raman effect in both liquid and solid $H_2$. Although previous spectra of both normal and pure parahydrogen have been reported,[2] only the semiquantitative values of the line*width* were obtained. Detailed studies of line shapes either as a function of ortho concentration or over a sufficient dynamic range have so far not been reported.

We have made measurements of the $\Delta J = 2$ pure rotational transitions $S_0(0)$ ($J=0\rightarrow 2$) and $S_0(1)$ ($J=1\rightarrow 3$) in both liquid and solid phases of ortho-parahydrogen mixtures, whose para concentration ranged between 25% and 96%. Using logarithmic display these spectra are examined far out into the wings (to ~$10^{-4}$ of the line-center intensity) where asymmetries and concentration, temperature, and liquid-solid effects are quite evident. We argue that the line shapes are dominated by two relatively independent types of interactions, which govern, respectively, the low- and high-frequency regimes. We present quantum calculations of the low-frequency mechanism—essentially an electric quadrupole-quadrupole molecular pair interaction—through its contribution to the second frequency moment of the rotational line shape. These results are found to compare favorably in both absolute magnitude and concentration dependence with experimental observations. The high-frequency tails are interpreted in the solid as due to phonon sidebands, and in the liquid to a generalization of this, in a manner similar to the previously established[3] relation between two-phonon Raman scattering in the solid and intermolecular scattering in the liquid. As expected from this viewpoint the high-frequency tails of the liquid lines are relatively insensitive to changes in the mixture concentration or temperature.

## II. EXPERIMENTAL DETAILS AND OBSERVATIONS

The experimental apparatus has been described elsewhere.[4] All Raman spectra were obtained using 40–200 mW of 4880-Å argon-laser excitation; the lower powers being necessary to preserve isothermal conditions in the solid samples. Temperature was monitored by a calibrated carbon resistor imbedded in the cell wall. In the liquid

experiments the vapor pressure was monitored and served as a more accurate measure of temperature. Temperature accuracy of $<0.1°K$ was easily achieved. Parahydrogen was prepared by liquifying normal hydrogen in the presence of a ferrous oxide catalyst. Concentrations of the samples were determined *in situ* spectroscopically from the ratio $\mathcal{R}$ of the integrated intensities of the $S_0(0)$ to the $S_0(1)$ lines. If $C$ is the fractional parahydrogen concentration, then[5]

$$C = \tfrac{3}{5}\mathcal{R}(1+\tfrac{3}{5}\mathcal{R})^{-1}.$$

### A. Concentration effects

Figure 1 presents an over-all view of the spectral and concentration ranges explored here. In the range 0–650 $cm^{-1}$ three features are evident in both the 25% [1(a)] and 96% [1(b)] $pH_2$ liquid spectra: the $S_0(1)$ ($J=1\rightarrow 3$) line at 586 $cm^{-1}$, the $S_0(0)$ ($J=0\rightarrow 2$) line at 353 $cm^{-1}$, and the low-frequency (0–250 $cm^{-1}$) spectrum, consisting of the $J=1\rightarrow 1$ tail out to ~40 $cm^{-1}$ in 1(a) and the intermolecular scattering which is present in both spectra, but more clearly evident as a broad critically damped peak around 100 $cm^{-1}$ in 1(b). Figure 1(c) covers the same spectral region in solid nearly pure parahydrogen. Both $\Delta J=2$ rotational transitions are clearly evident; however, the high-frequency tail is easily identifiable as a phonon sideband in contrast to the structureless wing for the liquid in 1(b). The first-order Raman-active zone-center TO mode at 38 $cm^{-1}$ is of course present in the solid but absent in the liquid.

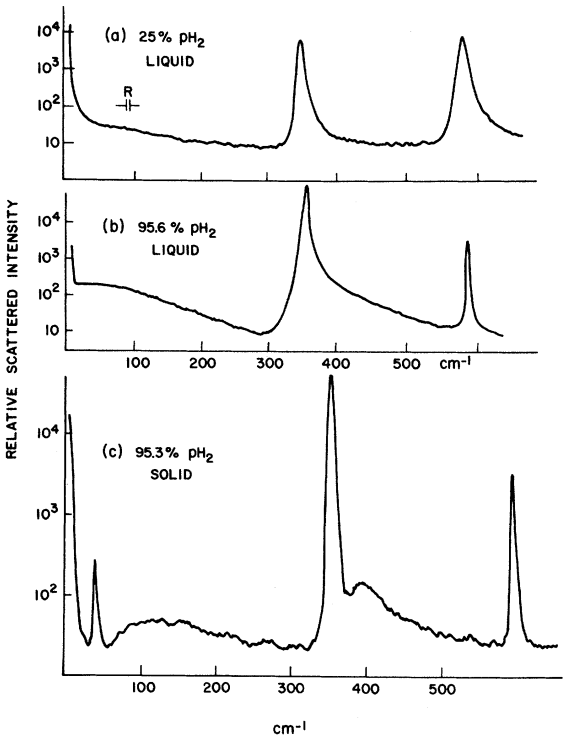


FIG. 1. Overview spectra of intermolecular and pure rotational scattering in condensed hydrogen. (a) Normal liquid hydrogen, $C_{para}=25\%$, $T=20.5$ °K; (b) liquid, $C_{para}=95.6\%$, $T=22.5$ °K; (c) solid, $C_{para}=95.3\%$, $T=11$ °K. Note logarithmic intensity scale. $R$ indicates instrumental full width at half-maximum.

Our previous work[3] concentrated on the low-frequency ($<300$ $cm^{-1}$) spectral range and showed the relation between the second-order Raman spectrum of the solid and the intermolecular scattering in the liquid. It was concluded that: (i) the intermolecular scattering provides evidence for relatively well-defined short-wavelength collective excitations in liquid $H_2$, which are essentially independent of ortho/para concentration and which are the remnants of zone-boundary phonon modes in the solid, and (ii) these collective translational excitations are at most weakly coupled to the rotational excitation ($J=1\rightarrow 1$). It was noted in that work, however, that all three rotational transitions exhibited marked line-shape dependence upon increasing ortho concentration and that the $\Delta J=2$ transitions in the solids were accompanied by weak—but clearly identifiable—phonon sidebands. As we will see below the far wings of these solid phonon sidebands are nearly identical in shape and intensity to the corresponding far wings in the liquid state.

Let us first present the low-frequency behavior since it exhibits the most marked concentration dependence. Figures 2 and 3 show higher resolution spectra of the $S_0(0)$ ($J=0\rightarrow 2$) and $S_1(0)$ ($J=1\rightarrow 3$) lines, respectively, at various parahydrogen concentrations between 25% and 95%, mostly at 14–15°K. Note that the spectra are plotted on a logarithmic intensity scale, with typically more than three decades of dynamic range exhibited within $\pm 10$ $cm^{-1}$ of the line center. Two general features are obvious upon increasing ortho concentration: the lines broaden and they develop evident asymmetries. The Stokes/anti-Stokes asymmetry about the line center is observed to be $e^{-\hbar\Delta\omega/kT}$, where $\Delta\omega=\omega-\omega_{S_0(i)}$, $i=0,1$. This is not as expected for homogeneously broadened spectral lines and suggests that the observed line broadening results from emission (anti-Stokes) and absorption (Stokes) of thermally generated excitations accompanying the rotational transition.

Since the $S_0(0)$ and $S_0(1)$ transitions take place, respectively, on para ($J=0$) and ortho ($J=1$) molecules in a relatively localized fashion, the line-shape variation with ortho concentration is a measure of the effect of the increasingly anisotropic ortho environment on the energy levels of both para and ortho molecules. Note that when $C_{ortho}\rightarrow 0$

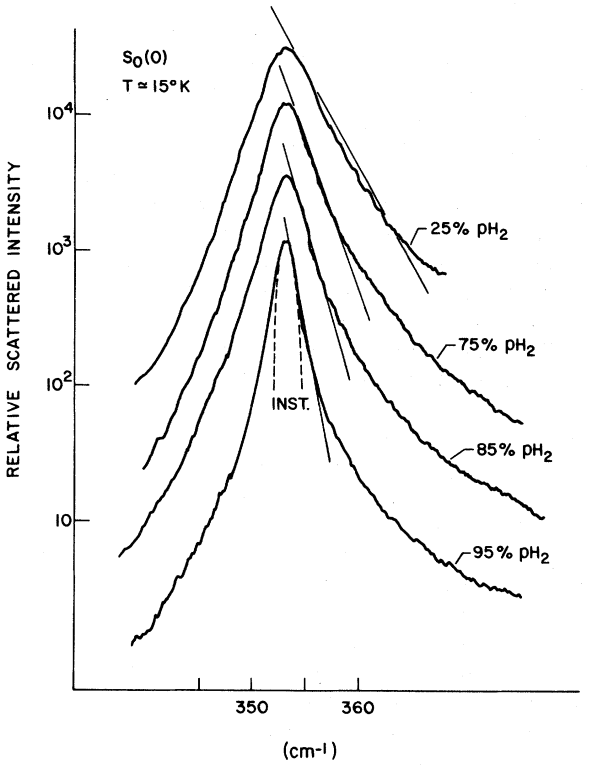


FIG. 2. High-resolution liquid spectra of $S_0(0)$ line shapes for various para concentrations. Spectra are vertically displaced on logarithmic intensity scale for display purposes. Straight lines illustrate determination of $\gamma$ as discussed in text.

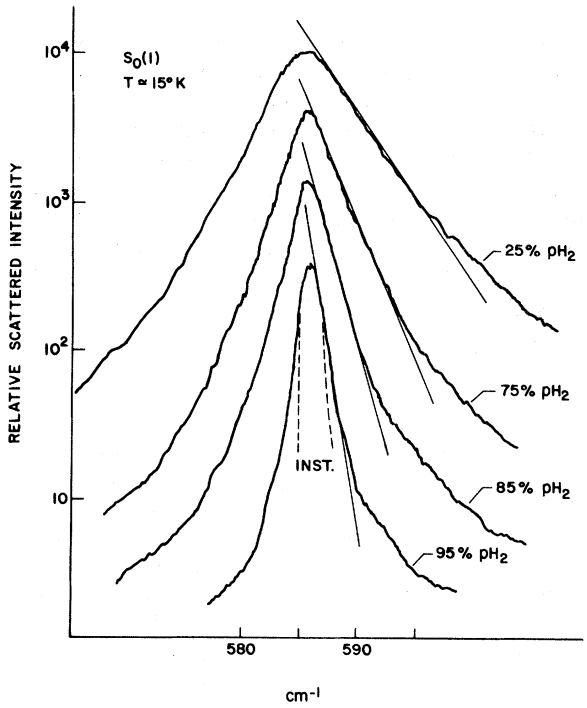


FIG. 3. High-resolution liquid spectra of $S_0(1)$ line shapes for ortho-para hydrogen mixtures. Notations are as in Fig. 2.

the linewidths of both transitions tend toward zero; but that as $C_{\text{ortho}}$ increases $\Delta\nu_{1\to3}$ increases more rapidly than does $\Delta\nu_{0\to2}$.

These results are summarized in Fig. 4, which shows the approximate second frequency moments $M_2$ (obtained as described in detail in Sec. IV) plotted against $C_{\text{ortho}}$. Note the consistency with a linear dependence on $C_{\text{ortho}}$.

Although not explicitly displayed here, we observed that for all concentrations studied here the shape of the quasielastic $\Delta J = 0,1 \to 1$ transition was very close to that of the $\Delta J = 2,1 \to 3$ transition, once the concentration-independent intermolecular scattering was subtracted.[3] The theory presented in Sec. III correctly predicts this similarity.

Although Bhatnagar *et al.*[2] exhibit no spectra for the liquid $S_0(0)$ and $S_0(1)$ transitions, they quote Raman "half-widths" of 3.5 and 4.5 $cm^{-1}$, respectively, for these transitions in normal hydrogen at approximately 18°K. Our data show *full widths* at half-maximum (FWHM) of 3.5 and 4.5 $cm^{-1}$ for these transitions at 20.2°K, obtained by *direct* subtraction of the instrumental width (1.5 $cm^{-1}$) from the total FWHM. Figures 2 and 3 show that

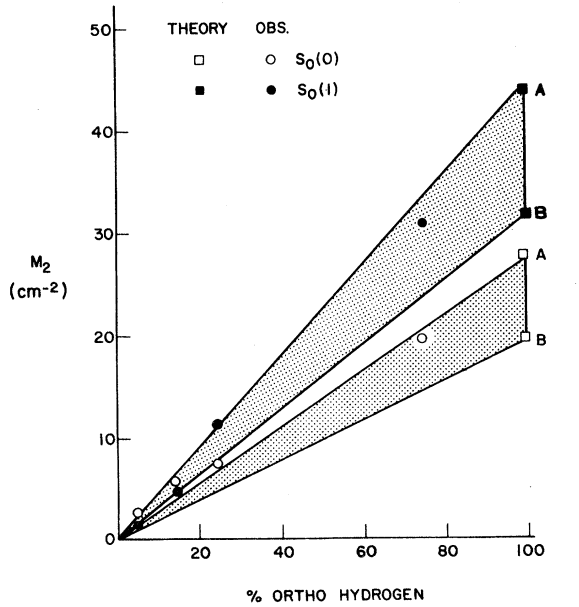


FIG. 4. Calculated and observed second moments of $S_0(0)$ and $S_0(1)$ spectra as function of ortho concentration. Shaded areas are determined as discussed in text.

the line shapes are definitely not Lorentzian and that they can be reasonably approximated by an exponential over the first decade and a half of the intensity drop off from the line center. Beyond this region the spectra fall off much more slowly and show negligible concentration dependence. We associate the latter behavior with the "quasiphonon" sideband region.

To motivate this association consider Fig. 5 showing the $S_0(0)$ transition in 95% parahydrogen in both the solid and liquid states. Note in the solid spectrum that the high-frequency side of the main 353-$cm^{-1}$ line exhibits a nonmonotonic sideband with a peak displaced by approximately 40 $cm^{-1}$. This coincides almost exactly with the dominant feature in the phonon density of states for solid $pH_2$ inferred by incoherent-neutron-scattering experiments[6] but differs appreciably from the density of states calculated by Nielsen,[7] which shows a second even more pronounced peak at ~65 $cm^{-1}$. The absence of this latter peak in both light and neutron scattering spectra is not completely understood, but appears related to the quantum nature of solid hydrogen. Phonon sidebands have not been observed previously in hydrogen Raman spectra probably due to their low intensities (~$10^{-3}$) relative to the main transitions.

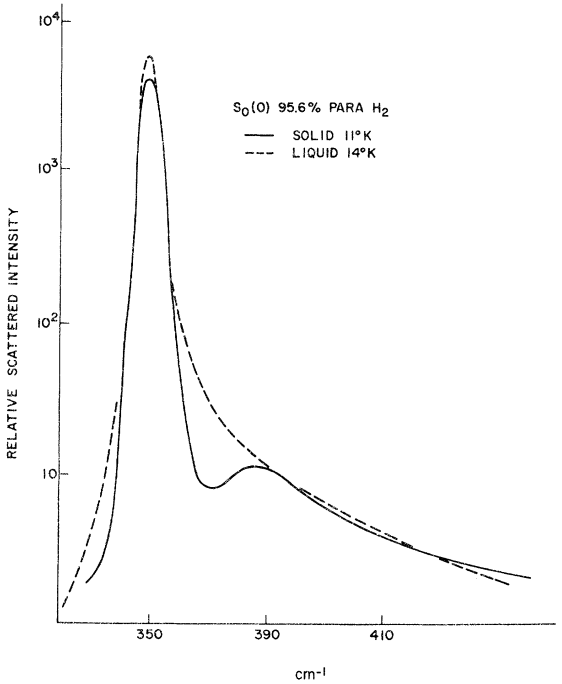


FIG. 5. Comparison of $S_0(0)$ line shapes for 95% parahydrogen in liquid (14 °K) and solid (11 °K) phases. Note similarity in far wings and clear peak representing solid phonon sideband at ~395 $cm^{-1}$.

Similarly, although considerable calculation has been done for the phonon sidebands of *infrared* absorption spectra in hydrogen,[8] none has been carried out for the Raman sidebands.

The similarity in far-wing line shapes between the liquid and solid spectra is clear in Fig. 5 indicating that in the liquid essentially the same mechanism is involved, even though the short-wavelength phonons, which dominate the sideband structure in the solid, are less well defined in the liquid state.

Since the phonon density of states depends mainly on isotropic interactions which are nearly independent of ortho-para composition, the above argument suggests that the far wings of the liquid spectra should not depend appreciably on $C_{\text{ortho}}$, in contrast to the near-wing behavior shown in Figs. 2 and 3. This independence of concentration is indeed observed.

### B. Temperature effects

The final aspect of experimental observations to be considered is the effect of temperature variation on the rotational Raman line shapes in the liquid. The "temperature dependence" of the spectra associated with the solid-liquid-phase change has already been discussed above.

Again it is convenient to distinguish two frequency regimes: the near ($\lesssim$ 30 $cm^{-1}$) and far ($\gtrsim$ 30 $cm^{-1}$) wings. Figure 6 shows clearly that the near wings of both the $S_0(0)$ and $S_0(1)$ lines at the same (85% para) concentration are considerably narrowed upon the ~57% increase in temperature from 14 to 22°K. In particular, the approximate widths—as determined from the exponent "$\gamma$" describing the near-wing intensity fall off $I(\omega) = I_0 e^{-(\omega/\gamma)}$—are 1.75 and 1.15 $cm^{-1}$ for $S_0(0)$ at 14 and 22°K, respectively, and 1.62 and 0.99 $cm^{-1}$ for $S_0(1)$ at 14 and 22°K, respectively.

It is clear from Fig. 7, which shows the $S_0(0)$ spectrum over a much wider frequency range, that there is virtually no temperature or concentration effect on the far wing (> 30 $cm^{-1}$). Similar temperature and concentration independence is observed in the far wings of $S_0(1)$ spectra.

## III. MOLECULAR PAIR ELECTRIC QUADRUPOLE-QUADRUPOLE INTERACTIONS

First-principles calculations of Raman line shapes in liquids would require a microscopic dynamical theory of the liquid state, which so far does not exist. Liquid hydrogen, however, provides a unique opportunity for at least a partial calculation because the hydrogen molecular wave functions and molecular pair interaction potential are well known. In this section we describe a cal-

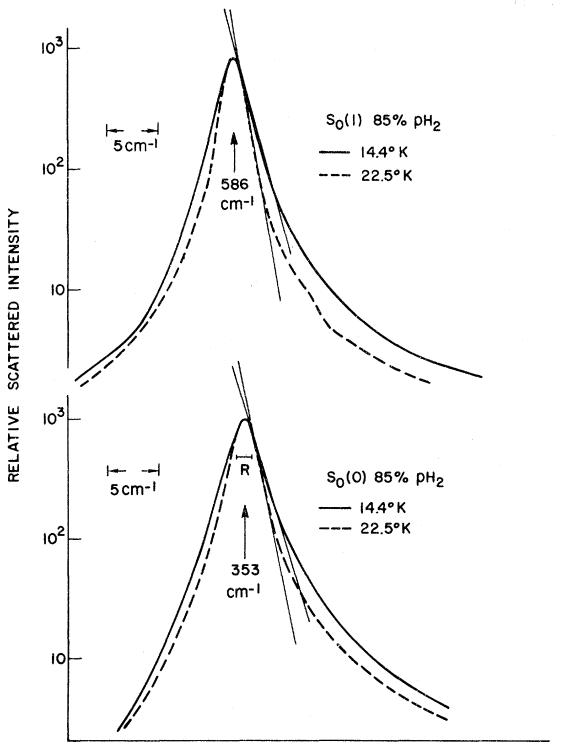


FIG. 6. High-resolution spectra of $S_0(0)$ and $S_0(1)$ lines in 85% parahydrogen emphasizing effect of temperature on near-wing lineshape. Superimposed straight lines determine the exponent $\gamma$.

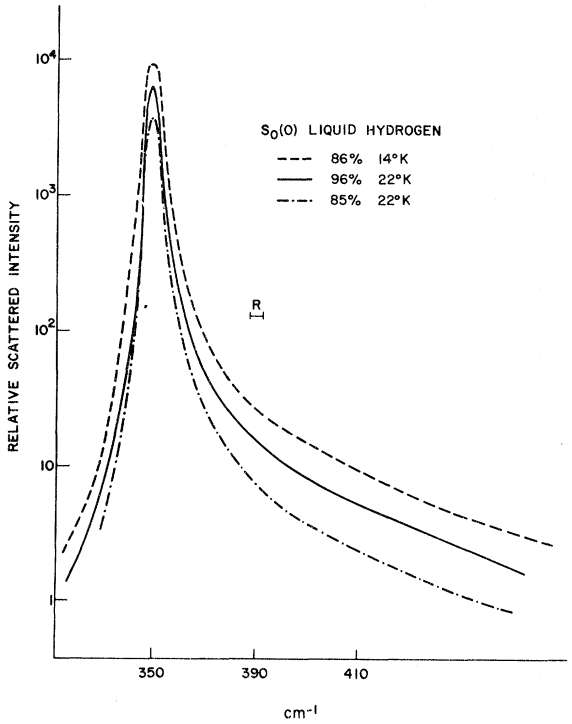


FIG. 7. Comparison of far-wing spectra of $S_0(0)$ lines in 85% parahydrogen at 14 and 22 °K, and in 96% parahydrogen at 22 °K. Note identity of high-frequency shapes.

culation of the second frequency moments of the rotational transitions under the following assumptions: (i) The intermolecular interaction is via the electric quadrupole-quadrupole coupling; (ii) molecular centers are fixed so that translation-rotation coupling is ignored; (iii) the polarizabilities of a pair of molecules are additive; and (iv) high-temperature approximations may be used in computing thermal averages.

In the absence of anisotropic interactions the rotational transitions $\Delta J = 0,2$ ($J = 1 \rightarrow 1, J = 0 \rightarrow 2$, $J = 1 \rightarrow 3$) would all be sharp concentration-independent lines of energies

$$E = \hbar\omega_{if} = B[J_f(J_f+1) - J_i(J_i+1)], \tag{1}$$

where $B$ is the rotational constant

$$B = \hbar^2/2Ic = 60 \text{ cm}^{-1} \text{ for } H_2$$

and $I$ is the moment of inertia. The presence of anisotropic terms in the intermolecular potential, however, removes the degeneracy of the levels originally characterized by the quantum numbers $J, m_J$. The strength of the anisotropic interactions is small compared with the spacing between $J$ levels, so the predominant effect is to cause a broadening of each $J$ level, which is no longer characterized by $m_J$.

The dominant anisotropic interaction at typical liquid and solid densities is known to be of the molecular electric quadrupole-quadrupole (EQQ) form[9]

$$\mathcal{H}_{EQQ} = 20\pi\Gamma \sum_m a_m Y_{2m}(\Omega_1) Y_{2-m}(\Omega_2), \tag{2}$$

$$a_0 = 1, \quad a_{\pm 1} = \tfrac{2}{3}, \quad a_{\pm 2} = \tfrac{1}{6},$$

where the $Y_{lm}$ are spherical harmonics and the $\Omega_i$ are measured relative to the intermolecular axis. Here the strength of the interaction is characterized by the EQQ coupling constant $\Gamma = \frac{6}{25} \times (e^2Q^2/R_{12}{}^5)$, where $eQ$ is the molecular electric quadrupole moment and $R_{12}$ is the distance between molecular centers. In Eq. (2) the quantization axis has been chosen as the intermolecular vector.

### A. $M_2$ for interacting pairs

Before discussing the rotational Raman spectra in condensed phases, it is instructive to examine the simplest case; namely, two $H_2$ molecules whose molecular centers are held rigidly at a distance $R$ apart. The scattered spectral intensity is given by Fermi's golden rule:

$$I(\omega) = \hbar^{-1} \sum_{i,f} P_i |\langle f|\alpha|i\rangle|^2 \delta(E_f - E_i - \hbar\omega). \quad (3)$$

The sum is over final states $f$ and initial states $i$ weighted by their thermal population factors $P_i$. For pure rotational spectra, the polarizability transition matrix elements of linear molecules are proportional to the anisotropy of the molecular polarizability $\beta = \alpha_\parallel - \alpha_\perp$, and are given in the spherical basis by

$$\alpha_q^{(2)}(j) = (\tfrac{4}{5}\pi)^{1/2} \beta Y_{2q}(\Omega_j). \quad (4)$$

To a first approximation the polarizabilities of a pair of molecules $j, k$ are additive:

$$\alpha_q^{(2)}(\text{pair}) = (\tfrac{4}{5}\pi)^{1/2} \beta [Y_{2q}(\Omega_j) + Y_{2q}(\Omega_k)]. \quad (5)$$

The components of $\alpha$ which contribute to a given spectrum are controlled by the polarization of the incident and scattered light. For example, if the incident and scattered light are both $z$ polarized only the $\alpha_{zz}(\text{lab})$ components are required:

$$\alpha_{zz}(\text{lab}) = (\tfrac{4}{5}\pi)^{1/2} \beta Y_{20}(\Omega_{\text{lab}}) = \alpha_0^{(2)}(\text{lab}). \quad (6)$$

This is related to the components $\alpha_q^{(2)}(\text{MFF})$ in the molecular fixed frame (MFF) by a Wigner rotation matrix,

$$\alpha_0^{(2)}(\text{lab}) = \sum_\mu \mathfrak{D}_{0\mu}^{(2)}(\alpha\beta\gamma) \alpha_\mu^{(2)}(\text{MFF}). \quad (7)$$

Similar considerations hold for the $\alpha_{xy}$, $\alpha_{zx}$, etc. components. In fact since the rotational spectra are completely depolarized, all spectra are related by simple geometric factors. It therefore suffices to consider only $\alpha_{zz}$ which is the simplest to evaluate.

In order to calculate the rotational spectra it remains to identify the initial and final pair rotational states and their energies. In the absence of anisotropic interactions, the individual molecular states are characterized by the quantum numbers $j$ and $m$ with wave functions given by the spherical harmonics $|j_i m_i\rangle = Y_{2m}(\Omega_i)$ and energies $E = Bj_i(j_i+1)$. The energy of a pair of molecules 1,2 would then be $E_{1,2} = E_1 + E_2$ with product states $|j_1 m_1\rangle |j_2 m_2\rangle$.

These product states are most conveniently considered in the coupled representation $|j_1 j_2 j m\rangle$, where $\vec{j} = \vec{j}_1 + \vec{j}_2$, and $m = m_1 + m_2$. The coupled states are related to the product states by the well-known prescription for the coupling of angular momenta[10]

$$|j_1 j_2 j m\rangle = (-1)^{j_2 - j_1 - m} \sum_{m_1 m_2} (2j+1)^{1/2} \begin{pmatrix} j_1 & j_2 & j \\ m_1 & m_2 & -m \end{pmatrix} \times |j_1 m_1\rangle |j_2 m_2\rangle. \quad (8)$$

$\begin{pmatrix} j_1 & j_2 & j \\ m_1 & m_2 & -m \end{pmatrix}$ is a 3-$j$ symbol. Here we have neglected resonance; that is, we have assigned particular values for the magnitudes of the angular momenta, $j_1$ to one particular molecule, and $j_2$ to the other, rather than allowing the rotational excitations to be mobile. This resonance is negligible, for our purposes, if the two molecules are of different parity (e.g., $j_1 = 2$, $j_2 = 1$), since excitational hopping then requires a simultaneous nuclear-spin flip; but if both molecules have the same parity (e.g., 1,3 or 0,2) exchange may be significant, as discussed below.

The presence of the quadrupole interaction mixes the $j$ states, but since there is isotropy about the intermolecular vector, $m$ is still a good quantum number, and it is convenient to carry out calculations in the $|j_1 j_2 j m\rangle$ basis. The energies and eigenfunctions can be characterized by the labels $\lambda$ and $m$

$$\mathcal{H}_{\text{EQQ}} |j_1 j_2 \lambda m\rangle = E_{j_1 j_2 \lambda m} |j_1 j_2 \lambda m\rangle, \quad (9)$$

where

$$|j_1 j_2 \lambda m\rangle = \sum_j C_{\lambda m j} |j_1 j_2 j m\rangle. \quad (10)$$

The convenience of working in the coupled angular momentum (CAM) representation results from the form of the EQQ interaction, Eq. (2). van Kranendonk[11] and Nakamura[9] have noted that in the CAM representation it has the symmetry of the fourth rank irreducible tensor $T_{40}$. To determine the energies and eigenfunctions we need then only diagonalize the matrices

$$\langle j_1 j_2 j' m | \mathcal{H}_{\text{EQQ}} | j_1 j_2 j m\rangle = D_{j_1 j_2} \langle j' m | Y_{40} | j m\rangle = D_{j_1 j_2} (-1)^m \left(\frac{(2j+1)(2j'+1)9}{4\pi}\right)^{1/2} \begin{pmatrix} j' & 4 & j \\ -m & 0 & m \end{pmatrix} \begin{pmatrix} j' & 4 & j \\ 0 & 0 & 0 \end{pmatrix}. \quad (11)$$

This matrix is block diagonal, since only at most three $j$ states with the same value of $m$ can mix. The coefficients $D_{j_1 j_2}$ can be evaluated directly for the special cases $j = j_1 + j_2$, $m = j_1 + j_2$, which do not mix with any others, giving

$$D_{11} = 14\pi^{1/2}\Gamma,$$

$$D_{21} = \tfrac{1440}{147}\pi^{1/2}\Gamma \approx 9.80\pi^{1/2}\Gamma,$$

$$D_{31} = \tfrac{715}{81}\pi^{1/2}\Gamma \approx 8.83\pi^{1/2}\Gamma.$$

A further simplification results from the fact that for $j_1, j_2 = 0$ or 1 the matrix is already diagonal. That is, the initial states of the system are properly labeled $|j_1 j_2 j m\rangle$.

The simplest characterization of a spectral line is in terms of its central frequency, or first moment, and its mean square frequency width or second moment $M_2 = \langle \omega^2 \rangle$. For a pair of molecules 1,2 in which molecule 1 undergoes the transition $j_1 \rightarrow j_1'$, we write

$$M_2(1,2,j_1,j_1') = \frac{\sum_{jm} P_{jm} \sum_{\lambda m'} |\langle j_1' j_2 \lambda m' | \alpha_0^{(2)}(\text{lab}) | j_1 j_2 j m \rangle|^2 (E_{j_1' j_2 \lambda m'} - E_{j_1 j_2 j m})^2}{\sum_{jm} P_{jm} \sum_{\lambda m'} |\langle j_1' j_2 \lambda m' | \alpha_0^{(2)}(\text{lab}) | j_1 j_2 j m \rangle|^2} . \tag{12}$$

In the high-temperature limit $kT \gg \Gamma$, there is no orientational correlation between molecules on the average, so all the $P_{jm}$ are equal, and can conveniently be set to 1. It remains to evaluate the polarizability matrix element

$$\begin{aligned} \mathcal{P} &= \langle j_1' j_2 \lambda m' | \boldsymbol{\alpha}_0^{(2)}(\text{lab},1) + \boldsymbol{\alpha}_0^{(2)}(\text{lab},2) | j_1 j_2 j m \rangle \\ &= \sum_{j'} C^*_{\lambda m' j'} \langle j_1' j_2 j' m' | \alpha_0^{(2)}(\text{lab},1) + \alpha_0^{(2)}(\text{lab},2) | j_1 j_2 j m \rangle . \end{aligned} \tag{13}$$

In the molecular fixed frame this becomes, using Eq. (7),

$$\mathcal{P} = \sum_{j'} C^*_{\lambda m' j'} \sum_{\mu} \mathfrak{D}^{(2)}_{0\mu}(\alpha\beta\gamma) \langle j_1' j_2 j' m' | \alpha_\mu^{(2)}(\text{MFF},1) + \alpha_\mu^{(2)}(\text{MFF},2) | j_1 j_2 j m \rangle . \tag{14}$$

The orientational average of the absolute square of $\mathcal{P}$ is particularly simple because of the orthogonality of the $\mathfrak{D}^{(2)}_{0\mu}$:

$$\int d\Omega \, \mathfrak{D}^{(2)}_{0\mu} \mathfrak{D}^{(2)}_{0\mu'} = \tfrac{8}{5} \pi^2 \delta_{\mu\mu'} . \tag{15}$$

After some rearrangement, we then have that

$$|\mathcal{P}|^2 = \frac{8\pi^2}{5} \left| \sum_{\mu j'} C^*_{\lambda m' j'} \langle j_1' j_2 j' m' | \alpha_\mu^{(2)}(\text{MFF},1) + \alpha_\mu^{(2)}(\text{MFF},2) | j_1 j_2 j m \rangle \right|^2 . \tag{16}$$

Since the $\alpha_\mu^{(2)}$ are given in the uncoupled single molecule basis, whereas the initial and final states are in the CAM representation a relationship must be found for the matrix element in the two bases. This can be done using Eq. (7.1.7) of Edmonds,[10] giving

$$\begin{aligned} \langle j_1' j_2 j' m' | \alpha_\mu^{(2)}(\text{MFF},1) + \alpha_\mu^{(2)}(\text{MFF},2) | j_1 j_2 j m \rangle &= (1+\delta_{j_1 j_1'})(-1)^{(j_2+2-m)} [(2j+1)(2j'+1)]^{1/2} \\ &\times \begin{Bmatrix} j_1' & j' & j_2 \\ j & j_1 & 2 \end{Bmatrix} \begin{pmatrix} j' & 2 & j \\ -m' & \mu & m \end{pmatrix} (j_1' \| \alpha^{(2)} \| j_1) . \end{aligned} \tag{17}$$

The large curly brackets represent a $6j$ symbol. The reduced matrix element $(j_1' \| \alpha^{(2)} \| j_1)$ appears in all terms of both the numerator and denominator of $M_2$ and thus need not be evaluated. Note that Eq. (17) gives $\mathcal{P}$ between a specific set of states $|j_1 j_2 j m\rangle \rightarrow |j_1' j_2 \lambda m'\rangle$.

The final form for the high-temperature limit of $M_2$ for a given transition $j_1 j_2 \rightarrow j_1' j_2$ can then be written as

$$M_2 = \mathfrak{N}/\mathfrak{D}, \tag{18}$$

where

$$\mathfrak{N} = \sum_{\lambda m'} \sum_{jm} |\mathcal{P}|^2_{jm \rightarrow \lambda m'} (E_{j_1' j_2 \lambda m'} - E_{j_1 j_2 j m})^2 , \tag{18a}$$

$$\mathfrak{D} = \sum_{\lambda m'} \sum_{jm} |\mathcal{P}|^2_{jm \rightarrow \lambda m'} . \tag{18b}$$

Explicit evaluation of Eq. (18) gives the values for the pair moments as listed in Table I. Note the similarity in the calculated values of the $|1,1\rangle \rightarrow |1,1\rangle$ and $|1,1\rangle \rightarrow |3,1\rangle$ moments, in agreement with the experimental observation in Sec. II A.

### B. $M_2$ in the condensed phases

Since, in the high-temperature limit, there is no orientational correlation between a central

TABLE I. Values for the pair moments $M_2$ for transitions $|j_1 j_2\rangle \rightarrow |j_1' j_2\rangle$.

| Transition $\lvert j_1 j_2\rangle \rightarrow \lvert j_1' j_2\rangle$ | Moment $M_2$ (units of $\pi\Gamma^2$) | Center frequency $\omega$ ($\text{cm}^{-1}$) |
|---|---|---|
| $\lvert 1,1\rangle \rightarrow \lvert 1,1\rangle$ | 4.44 | 0 |
| $\lvert 1,0\rangle \rightarrow \lvert 1,0\rangle$ | 0 | 0 |
| $\lvert 0,1\rangle \rightarrow \lvert 2,1\rangle$ | 2.73 | 353 |
| $\lvert 0,0\rangle \rightarrow \lvert 2,0\rangle$ | 0 | 353 |
| $\lvert 1,1\rangle \rightarrow \lvert 3,1\rangle$ | 4.40 | 586 |
| $\lvert 1,0\rangle \rightarrow \lvert 3,0\rangle$ | 0 | 586 |

molecule and its neighbors, the second moments are then pairwise additive. For $n$ neighbors all at the same intermolecular distance,

$$M_2(n) = n \times M_2(\text{pair}), \quad M_2(\text{pair}) \sim 1/R^{10}.$$

If the neighbors are distributed according to a distribution function $g(R)$, then

$$M_2(n) \approx 4\pi \frac{N}{V} \int g(R) R^{-8}\, dR.$$

Since this drops off quite rapidly with $R$, we include in our estimate only the first-neighbor shell. This gives, for example,

$$M_2(j=1 \to 3) = n(1-X) M_2(R)(1,0 \to 3,0) + nX M_2(R)(1,1 \to 3,1).$$

where $X$ is the mole fraction of $J=1$ molecules, $M_2(R)$ is the pair moment evaluated at the distance $R$, and $n$ is the number of nearest neighbors.

## IV. DISCUSSION

In order to evaluate $M_2$ in the condensed phase for comparison with experiment, values for $n$, the number of nearest neighbors, and $\Gamma$, the EQQ interaction strength, are required. In the solid these are known[12] to be $n=12$ for hexagonal-close-packed structure, and $\Gamma = 0.551$ cm$^{-1}$ at the 4.2 °K solid density of 22.8 cc/mole. Since no detailed measurements of the liquid-state structure factor $S(q)$ exist for liquid hydrogen, $n$ is not accurately known. Similarly, the value for the effective nearest-neighbor distance $R$, which determines $\Gamma$ through the relation $\Gamma = \frac{6}{25}(e^2Q^2/R^5)$, is not known. Therefore, we have evaluated $M_2$ for two simple limiting cases: (A) the value of $\Gamma$ in the liquid is the same as in the solid and the effective number of nearest neighbors is scaled according to the liquid density (26.25 cc/mole at the triple point) and (B) the number of liquid nearest neighbors is the same, 12, as in the solid and the interaction $\Gamma$ is scaled as the density change between solid and liquid.

Assumption (A) implies that since $\rho_{\text{solid}} = 1.15\rho_{\text{liq}}$, $n_{\text{liq}} = 0.87 n_{\text{solid}} = 10.4$. Therefore, $M_2$ equals 27.1 and 43.6 cm$^{-2}$, respectively, for the $S_0(0)$ and $S_0(1)$ moments in the 100% orthohydrogen limit. The $\Delta J = 0$, $(1 \to 1)$ moment is 44.1 cm$^{-2}$ at 100% ortho concentration. Assumption (B) requires $\Gamma_{\text{liq}} = (\rho_{\text{liq}}/\rho_{\text{solid}})^{5/3}\Gamma_{\text{solid}} = 0.435$ cm$^{-1}$ with $n_{\text{liq}} = n_{\text{solid}} = 12$. This yields values for $M_2$ of 19.5 and 31.4 cm$^{-2}$, respectively, for the $S_0(0)$ and $S_0(1)$ transitions in the pure-ortho limit. The $\Delta J = 0$ limiting moment is 31.7 cm$^{-2}$. Since we have neglected exchange interaction broadening, all moments will go to zero as $C_{\text{ortho}} \to 0$. It should be noted that the experimental second moment[13] of the $S_0(0)$ transition in pure solid para $H_2$, where the total linewidth is caused by resonance amounts to only ~2.2 cm$^{-2}$.

On Fig. 4 are plotted several experimental points for the frequency moments which were obtained from the spectra as follows. Only the high-frequency side of the line was considered, and the far wing ($\gtrsim 30$ cm$^{-1}$) was ignored. Over approximately the first decade of intensity decrease from the line center, the spectrum could be reasonably approximated by an exponential as estimated by the straight lines superimposed in Figs. 2 and 3. The second moment of such an exponential spectrum, $I(\omega) = I_0 e^{-\omega/\gamma}$, is just $2\gamma^2$. Within 2% this is equal to the square of the full width at half-maximum for an exponential spectrum. The influence of the far wings, which also may be approximated by an exponential of much higher characteristic frequency, on the experimental $M_2$ is typically less than 1%.

As can be seen from Fig. 4 the observed moments are in good agreement with a linear dependence on $C_{\text{ortho}}$, although the $S_0(0)$ line appears to extrapolate to a finite value of ~2 cm$^{-2}$ as $C_{\text{ortho}} \to 0$. While this may be a resonance effect, the determinations of $M_2$ are not sufficiently accurate to confirm this. Overall, the experimental values are in good absolute agreement with the calculations, falling particularly close to those based on a model in which the nearest neighbors in the liquid pack at about the same distance apart as in the solid, and that the lower density of the liquid is most simply considered as reflecting a lowering of the coordination number. This is consistent with direct determination of the radial distribution function of classical liquids such as argon, by neutron[14] and x-ray scattering.[15] Unfortunately, there have been no measurements of the radial distribution function in liquid $H_2$ with which to compare.

The overall good agreement also tends to substantiate the validity of the high-temperature approximation for the orientational distribution in the liquid. We note that the orientational ordering temperature of pure ortho hydrogen is 2.8 K, while the liquid range is more than a factor of 5 higher.

### Far wing

The far wings of both lines are apparently determined by the liquid-state generalization of what in the solid constitutes a phonon sideband. While such features have not been reported before in the Raman spectra of hydrogen, they are in fact the dominant contributors to the infrared absorption.[16] The liquid-solid differences and similarities evident in the Raman spectra of Fig. 5 are qualitatively reminiscent of structure seen in the $Q$-branch absorption spectra near 4500 cm$^{-1}$. There are

however two major differences in the sideband spectra as observed by the Raman scattering and infrared-absorption techniques.

Most striking is the very much smaller intensities of the sidebands in the Raman effect than in the infrared absorption. This is due to two causes: (a) the main (zero-phonon) transition is Raman allowed and almost ir forbidden by the high crystal symmetry and (b) intermolecular motions merely cause a small change in the already appreciable polarizability which determines the Raman cross section; but are responsible for large induced dipole moments which determine the ir absorption coefficient. Typically, the phonon sidebands in ir spectra of solid hydrogen are several times stronger than the main absorption; whereas Fig. 5 shows the Raman sideband nearly 500 times weaker than the main line. This difference may account for the lack of theoretical attention paid to phonon sidebands in Raman spectra despite their potentially simpler interpretation, than is encountered in the infrared.

The second major difference lies in the observed sideband shape. Above it was noted that the sideband in Fig. 5 is peaked at ~40 $cm^{-1}$ from the main transition and agrees with the observed shape of the phonon density of states for solid $H_2$.[5] The ir spectra of Gush *et al.*[16] which have been interpreted as sidebands to the $S_1(0)$ transition at 4486 $cm^{-1}$, peak at ~65 $cm^{-1}$ frequency displacement. In pure para $H_2$ a much weaker peak was also observed at ~42 $cm^{-1}$. It is possible that selection-rule processes emphasize different regions of the Brillouin zone for sideband spectra in Raman scattering and in ir absorption. It might also be that the ir sidebands mentioned above really belong to the relatively sharp $[Q_1 + S_0(0)]$ feature centered at 4505 $cm^{-1}$. This would lower the "phonon" frequencies by 19 $cm^{-1}$ and bring the "densities of states" observed by the two techniques into agreement.

A crude estimate of the scattering efficiency in the phonon sideband relative to that of the main rotational transition can be obtained as follows. Both depolarized spectral features arise from the anisotropy of the polarizability $\beta$, which may be expanded as

$$\beta(R) = \beta_0 + (\partial\beta/\partial R)\delta R,$$

where the first term controls the pure rotational transition, and the second describes the effect of changing the intermolecular distance $R$, which gives rise to a translational-rotational transition.

Considering the polarized components $I_{zz}$ only, we note $I_{zz}(S_0(0)) \simeq \frac{1}{5}\beta_0^2$. From the induced dipole theory of collision-induced (or translational-intermolecular) scattering[17]

$$I_{zz}(\text{coll. ind.}) = \frac{4}{45}\left(\frac{\partial\beta}{\partial R}\right)^2 \langle \delta R^2 \rangle ,$$

where $\langle \delta R^2 \rangle$ is the mean square molecular displacement (0.48 $Å^2$ for solid parahydrogen,[6]) and $\partial\beta/\partial R = 9\alpha_0^2/R^4$. Thus

$$a = \frac{I_{zz}(\text{coll. ind.})}{I_{zz}(S_0(0))} \simeq \frac{4}{45}\,\frac{81\alpha_0^4}{R^8}\langle \delta R^2 \rangle \frac{5}{\beta_0^2} .$$

Using[18] $\beta_0 = 0.22$ $Å^3$; $\alpha_0 = 0.79$ $Å^3$, $R = 3.75$ Å we find $a = 3.5 \times 10^{-3}$. The observed ratio evident in Fig. 5 is certainly of this order of magnitude. The "agreement" is probably to a large extent fortuitous and should only be taken as a suggestion that the mechanism considered is probably the dominant one. Clearly a detailed theoretical treatment for Raman sidebands of the type given by Poll and Van Kranendonk[8] for the ir case is now in order.

In conclusion we have presented a number of new aspects of the rotational Raman spectra in the condensed phases of ortho-para hydrogen mixtures of widely varying concentrations. We have demonstrated that this system provides a unique opportunity for detailed study of the dynamics of interactions among isotropic and anisotropic molecules which are chemically identical. A simple quantum-mechanical calculation of the second frequency moments for the $(1 \rightarrow 1)$, $(1 \rightarrow 3)$, and $(0 \rightarrow 2)$ rotational transitions has provided good agreement with the measured moments as regards both absolute magnitude and concentration dependence. The far-wing behavior of the line shapes has been identified in the solid as a phonon sideband, and in the liquid to a generalization of that concept. This identification suggests that from such far-wing behavior, something like a phonon density of states in a liquid may be inferred. Finally the present experimental data points out the need for more sophisticated theories of Raman line shapes in condensed hydrogen, similar to those already developed for infrared spectra.

ACKNOWLEDGMENTS

We are grateful to F. Hanson, J. Noolandi, and J. M. Worlock for helpful discussions, and to H. L. Carter and A. Kane for technical and computational assistance.

*That portion of the work done at U.C.L.A. supported in part by a grant from the National Science Foundation.

†Work performed as a Resident Visitor at Bell Laboratories.

‡Permanent address.

[1]See, for example, R. G. Gordon, J. Chem. Phys. 40, 1973, (1964); R. Callender and P. S. Pershan, Phys. Rev. A 2, 672 (1970).

[2]S. S. Bhatnagar, E. J. Allin, and H. L. Welsh, Can. J. Phys. 40, 9 (1962).

[3]P. A. Fleury and J. P. McTague, Phys. Rev. Lett. 31, 914 (1973).

[4]P. A. Fleury, J. M. Worlock, and H. L. Carter, Phys. Rev. Lett. 30, 591 (1973).

[5]I. F. Silvera, W. N. Hardy, and J. P. McTague, Discuss. Faraday Soc. 48, 54 (1970).

[6]H. Stein, H. Stiller, and R. Stockmeyer, J. Chem. Phys. 57, 1786 (1972).

[7]M. Nielsen (private communication).

[8]J. D. Poll and J. Van Kranendonk, Can. J. Phys. 40, 163 (1962).

[9]See, for example, T. Nakamura, Prog. Theo. Phys. Suppl. 46, 343 (1970).

[10]A. R. Edmonds, *Angular Momenta in Quantum Mechanics* (Princeton U. P., Princeton, N.J., 1957).

[11]J. Van Kranendonk, Can. J. Phys. 38, 240 (1960).

[12]I. F. Silvera, W. N. Hardy, and J. P. McTague, Phys. Rev. B 4, 2724 (1971).

[13]J. P. McTague, I. F. Silvera, and W. N. Hardy, in *Proceedings of the Second International Conference on Light Scattering in Solids*, edited by M. Balkanski, (Flammarion, Paris, 1971).

[14]G. D. Henshaw, Phys. Rev. 105, 976 (1957).

[15]P. G. Mikolaj and C. J. Pings, J. Chem. Phys. 46, 1401 (1967).

[16]H. P. Gush, W. F. Hare, E. J. Allin, and H. L. Welsh, Can. J. Phys. 38, 176 (1960).

[17]See, for example, J. P. McTague, W. D. Ellenson, and L. H. Hall, J. Phys. (Paris) 33, C1-241 (1972).

[18]J. O. Hirschfelder, C. F. Curtiss, and R. B. Bird, *Molecular Theory of Gases and Liquids* (Wiley, New York, 1954).